Myeloperoxidase Metabolizes Thiocyanate in a Reaction Driven by Nitric Oxide †

ARTICLE *in* BIOCHEMISTRY · FEBRUARY 2006

Impact Factor: 3.02 · DOI: 10.1021/bi051438k · Source: PubMed

Myeloperoxidase Metabolizes Thiocyanate in a Reaction Driven by Nitric Oxide†

Semira Galijasevic,‡ Ghassan M. Saed,‡ Stanley L. Hazen,‖ and Husam M. Abu-Soud*,‡,§

Department of Obstetrics and Gynecology, The C. S. Mott Center for Human Growth and Development, and Department of Biochemistry and Molecular Biology, Wayne State University School of Medicine, Detroit, Michigan 48201 and Departments of Cell Biology and Cardiovascular Medicine, Cleveland Clinic Foundation, Cleveland, Ohio 44195

Received July 21, 2005; Revised Manuscript Received October 19, 2005

ABSTRACT: We examined the potential physiological relevance of myeloperoxidase (MPO)−nitric oxide (NO) interactions as they may relate to the cosubstrate, pseudo halide thiocyanate (SCN^-), and substrate switching. Direct spectroscopic and rapid kinetics studies revealed that SCN^- interaction with MPO facilitates formation of the MPO catalytic intermediate Compound II, limiting overall activity. However, a physiological NO concentration (2 μM or less) dramatically influences the build-up, duration, and decay of the steady-state level of MPO Compound II during the metabolism of SCN^-, allowing the enzyme to function at full capacity. At higher NO concentrations, we observed significant increases in the rate of MPO Compound II formation, along with proportional increases in its duration as determined by the time elapsed during catalysis. Surprisingly, the decay rate of MPO Compound II remained unaltered as NO concentrations were increased. Computer simulations were carried out to model the kinetics of MPO Compound II formation, duration, and decay during the metabolism of SCN^- as a function of NO concentration. These simulation traces closely approximate what was observed experimentally and support the involvement of a conformational intermediate of MPO Compound II complex decay, altering the overall capacity of MPO to promote two electrons versus one-electron oxidation reactions during steady-state catalysis. Collectively, the present studies reveal that (patho)physiologically relevant levels of NO have significant effects on MPO Compound II accumulation. Thus, NO affects the overall rate of peroxidation of substrates and the overall ability of the peroxidase to execute one- versus two-electron oxidation reactions.

Myeloperoxidase (MPO),[1] an abundant protein found in neutrophils, monocytes, and selected tissue macrophages, plays an important role in generating an array of toxic oxidants important to host defenses (*1*). This heme-containing protein is expressed in the bone marrow and stored in leukocyte granules during granulocyte maturation (*1*, *2*). Upon phagocyte activation in peripheral blood, tissues, or fluids, MPO is released from leukocytes into both the phagolysosomal compartment and the extracellular milieu (*1*, *2*). MPO serves as an enzymatic catalyst of oxidatively modified tissues and is commonly implicated in numerous inflammatory diseases, including cardiovascular pathogenesis (*2*−*7*). MPO reacts rapidly with hydrogen peroxide (H_2O_2), generating MPO Compound I, a ferryl π cation radical (MPO−Fe(IV)═$O^{\bullet+\pi}$), which in turn oxidizes halides or pseudo halides through a single $2e^-$ transition into their corresponding hypohalous acids, which are all toxic to microbes (*8*, *9*). Alternatively, MPO Compound I can be reduced back to the ferric state through two successive $1e^-$ transfer reactions, generating radical species and the MPO intermediate Compound II (MPO−Fe(IV)═O) (*10*−*12*). Reduction of Compound II to the ferric state is thought to be the rate-limiting step in its classic peroxidase cycle, and this step can be accelerated by physiological reductants such as superoxide ($O_2^{\bullet-}$), nitric oxide (NO), and ascorbic acid (*13*−*15*). Previously, we have demonstrated that NO can both serve as a substrate for mammalian heme peroxidases as well as influence their catalytic activity (*15*−*18*). High levels of NO are inhibitory through the formation of a stable six-coordinate low-spin nitrosyl complex with the ferric heme, whereas low levels of NO accelerate the overall rate of the peroxidase cycle through reduction of Compounds I and II (*15*−*17*). We have also shown that the MPO−H_2O_2 system upregulates the catalytic activity of inducible nitric oxide synthase (iNOS) by scavenging NO, preventing feedback inhibition attributed to the formation of an iNOS−Fe−NO complex (*18*).

The pseudo halide thiocyanate (SCN^-) is a physiological substrate for the mammalian heme peroxidases (*19*, *20*). A relatively abundant anion in plasma, physiological SCN^- concentrations are typically in the range of 20−120 μM, depending upon the vegan content of the diet (*21*). Kettle

† This work was supported by the National Institutes of Health Grants HL066367, HL076491, HL70621.

* To whom correspondence should be addressed. Tel.: 313-577-6178; fax: 313-577-8554; e-mail: habusoud@med.wayne.edu.

‡ Department of Obstetrics and Gynecology, The C. S. Mott Center for Human Growth and Development, Wayne State University School of Medicine.

§ Department of Biochemistry and Molecular Biology, Wayne State University School of Medicine.

‖ Departments of Cell Biology and Cardiovascular Medicine, Cleveland Clinic Foundation.

[1] Abbreviations: MPO, myeloperoxidase; LPO, lactoperoxidase; EPO, eosinophil peroxidase; NO, nitric oxide (nitrogen monoxide); NOS, nitric oxide synthase; H_2O_2, hydrogen peroxide; SCN^-, thiocyanate.

10.1021/bi051438k CCC: $33.50
Published on Web 01/05/2006

and colleagues (*22*) reported that at physiological concentrations of halides (100 mM Cl^-, 50−150 μM Br^-, and 0.1−0.6 μM I^- (*23*−*25*), oxidation of SCN^- accounts for approximately 40% of H_2O_2 consumed by MPO. Recently, we have shown that incubation of SCN^- with MPO and other members of the mammalian peroxidase superfamily [e.g., eosinophil peroxidase (EPO) and lactoperoxidase (LPO)] causes multiple and sequential reactions through its potential capacity to act as a common substrate for the enzymes, a competitive inhibitor with respect to H_2O_2, or a ligand by binding to the heme iron (*26*). However, the direct reaction between MPO Compound I and SCN^- is extremely fast and occurred with an apparent second-order rate constant of 9.6×10^7 M^{-1} s^{-1} (*27*).

Plasma levels of SCN^- are markedly increased in tobacco smokers, reaching levels as high as 1.4−4.0 mM in saliva (*28*). Indeed, when SCN^- levels reach this high, its biochemical measurement is thought to serve as an objective indicator of tobacco consumption (*29*−*31*). SCN^- has been suggested to promote a decrease in endogenous NO formation (*29*−*33*). Similarly, we have recently demonstrated that MPO and other mammalian heme peroxidases can utilize NO as a substrate, serving to remove NO at sites of inflammation and in cardiovascular diseases (*15*−*18*). Detailed kinetic analyses examining the impact of NO and SCN^- on MPO steady-state catalysis have not yet been reported.

To further assess the potential physiological relevance of NO interactions with MPO under conditions that more closely mirror high-risk subjects, such as smokers, we investigated the effect of varying NO concentrations on MPO catalysis in the presence of plasma levels of SCN^- using stopped-flow and computer simulation methods. Our results revealed that addition of NO to MPO, H_2O_2, and SCN^- results in a significant increase in the levels of MPO Compound II accumulation during steady-state catalysis. Compound II, the rate-limiting intermediate in the peroxidase cycle, cannot readily use SCN^- as a substrate (SCN^- is normally a $2e^-$ acceptor and this $1e^-$ step is not favorable). Thus, an additional effect of NO on MPO catalysis is to influence the types of oxidation reactions available to the hemoprotein by modulating the distribution of intermediate forms during steady-state catalysis. This will have the net effect of promoting substrate switching, steering the MPO reaction from a $2e^-$ oxidation to a $1e^-$ oxidation pathway, by modulating substrate selectivity of the enzyme.

MATERIALS AND METHODS

Materials. NO gas was purchased from Matheson Gas products, Inc., and used without further purification. For each experiment, a fresh saturated stock of NO was prepared under anaerobic conditions. The extent of nitrite/nitrate (NO_2^-/NO_3^-) build-up in NO preparations over the time course used for the present studies was <1−1.5% (per mol NO), as determined by anion exchange HPLC under anaerobic conditions (*34*). All other reagents and materials were of the highest purity grades available and obtained from Sigma Chemical Co. (St. Louis, MO) or the indicated source.

General Procedures. MPO was initially purified from detergent extracts of human leukocytes by sequential lectin affinity and gel filtration chromatography (*35*). Trace levels of contaminating EPO were then removed by passage over a sulfopropyl Sephadex column (*36*). Purity of isolated MPO was established by demonstrating a Reinheitzal (RZ) value of >0.85 (A_{430}/A_{280}), SDS−PAGE analysis with Coomassie Blue staining, and gel tetramethylbenzidine peroxidase staining to confirm no contaminating EPO activity. Enzyme concentration was determined spectrophotometrically utilizing extinction coefficients of 89 000 M^{-1} cm^{-1}/heme of MPO (*37*). The concentration of the MPO dimer was calculated as half the indicated concentration of heme-like chromophore (*38*).

Optical Spectroscopy and Rapid Kinetic Measurements. Optical spectra were recorded on a Cary 100 Bio UV−visible spectrophotometer at 25 °C. Anaerobic spectra of MPO forms were recorded using septum-sealed quartz cuvettes that could attach through a quick-fit joint to a vacuum system. The peroxidase samples were made anaerobic by repeated cycles of evacuation and equilibrated with catalyst-deoxygenated N_2. Cuvettes were maintained under N_2 or NO atmosphere during spectral measurements. The kinetic measurements of MPO Compound II formation and decay in the absence and presence of different NO concentrations were performed using a dual syringe stopped-flow instrument obtained from Hi-Tech, Ltd. (model SF-61). Experiments were initially performed under conditions identical to those recently reported for MPO (*15*−*18*, *26*) to facilitate comparisons. Measurements were carried out under an anaerobic atmosphere at 10 °C following rapid mixing of equal volumes of an H_2O_2-containing buffer solution and a peroxidase solution that contained different NO concentrations. Reactions were monitored at both 432 and 455 nm. The time course of absorbance change was fit to the following: simple linear equation, single-exponential; ($Y = 1 - e^{-kt}$), or double-exponential ($Y = Ae^{-k_1 t} + Be^{-k_2 t}$) functions as indicated. Signal-to-noise ratios for all kinetic analyses were improved by averaging at least six to eight individual traces. In some experiments, the stopped-flow instrument was attached to a rapid scanning diode array device (Hi-Tech) designed to collect a multiple number of complete spectrum (200−800 nm) at specific time ranges. The detector was automatically calibrated relative to a holmium oxide filter, as it has spectral peaks at 360.8, 418.5, 446.0, 453.4, 460.4, 536.4, and 637.5 nm, which were used by the software to correctly align pixel positions with wavelength. Rapid scanning experiments involve mixing solutions of peroxidase (1−2 μM) preincubated with 200 μM SCN^- in the absence or presence of 5 μM NO with buffer solutions containing 40 μM H_2O_2, at 10 °C.

Solution Preparation. A fresh saturated stock of NO was prepared under anaerobic conditions. Anaerobic 0.2 M sodium phosphate buffer solutions, pH 7.0, containing various concentrations of NO were prepared by mixing different volumes of buffer saturated with NO gas at 21 °C with anaerobic buffer solution. A saturating concentration of NO at 21 °C is approximately 2 mM.

Model Simulations. The kinetic data collected from the stopped-flow were transferred to a Dell computer and, subsequently, processed with Reaction Kinetics Software (ChemSW; CA), using the comprehensive kinetic model that appears in Scheme 1. The rate constants that were used in the simulation process were either from experiments at 10 °C or were values from other experiments adjusted for temperature differences.

Scheme 1: Comprehensive Kinetic Model for NO and SCN^- Interactions with Myeloperoxidase

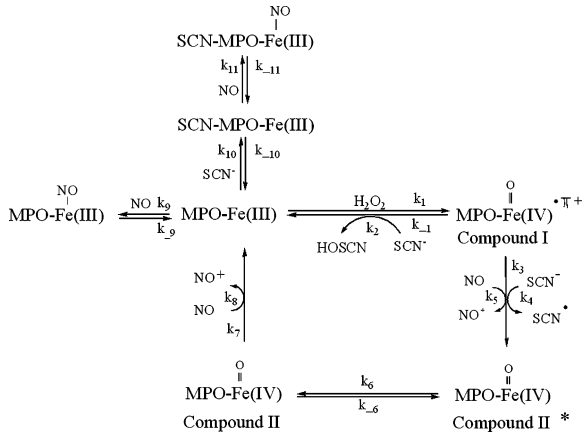

RESULTS

The reaction between MPO−Fe(III) and H_2O_2 generates Compound I, which was characterized by a significant decrease in the extinction coefficient of the Soret absorbance peak and a shift from 432 to 428 nm, as previously reported (*10*, *27*, *38*−*41*). The peroxidase intermediate formed within the first few milliseconds of initiating the reaction is unstable and is rapidly converted to a more stable peroxidase intermediate, Compound II (E−Fe(IV)═O), within the following several seconds (*10*, *23*, *38*−*41*). MPO Compound II displays a Soret absorbance peak centered at 455 nm and visible bands centered at 600 and 628 nm, typical of a six-coordinate complex. This intermediate is relatively stable and decays slowly to the ferric state in the next 500 s.

Rapid mixing of a solution of 1 μM MPO−Fe(III) preincubated with 200 μM SCN^- with an equal volume of a 40-fold molar excess of H_2O_2 resulted in rapid formation of MPO Compound II. Compound II formation occurred without any sign of MPO Compound I accumulation, and its build-up depended inversely on the SCN^- concentration used. For example, 90−95% of the enzyme converted rapidly to Compound II when MPO−Fe(III), the ferric state of the enzyme, was preincubated with 20 μM SCN^- before mixing with 40 μM H_2O_2, while 40−50% of the enzyme rapidly converted to Compound II when the enzyme was preincubated with 200 μM SCN^- before mixing with H_2O_2. Figure 1A, inset, shows the time course for the formation and decay of Compound II detected by monitoring the absorbance change at 455 nm, when a solution of 1 μM MPO preincubated with 200 μM SCN^- was rapidly mixed with 40 μM H_2O_2 utilizing a single wavelength stopped-flow spectrophotometer. The change in absorbance that takes place in the first 50 s of the reaction is shown in Figure 1A and is attributed to the build-up of Compound II content. Figure 1A shows spectra traces collected at 0.1, 2, 5, 20, and 42 s after initiating the reaction using a diode array spectrophotometer. The build-up of Compound II was best fit to a single-exponential function, giving an apparent pseudo first-order rate constant of 6.3 s^{-1}. The subsequent decrease in absorbance at 455 nm observed was best fit to a double-exponential function with rate constants of 1.0 s^{-1} for the faster phase, and 0.008 s^{-1} for the slower phase.

The addition of NO to the reaction mixtures results in dramatic effects on the rates of MPO Compound II build-up, duration, and decay, as assessed by direct absorbance and stopped-flow measurements (Figures 1 and 2, respectively). NO readily competed with SCN^- and was a $1e^-$ substrate for MPO Compound I that steered the reaction from a $2e^-$ oxidation of SCN^- to a $1e^-$ oxidation pathway. This behavior was assessed by the increased amplitude of the Soret absorbance peak at 455 nm, acceleration in the observed rate of MPO Compound II and decay, and shortening in the steady-state level. Figure 1B shows spectra collected at 0.01, 0.042, 0.13, 0.2, and 0.5 s after mixing a solution of 1 μM MPO preincubated with 200 μM SCN^- in the presence of 5 μM NO with 40 μM H_2O_2. Spectral transitions between MPO Compound II and the ferric state revealed distinct isosbestic points (data not shown). The appearance of one set of isosbestic points suggests that only two components were present, which, in this case, are MPO Compound II and the ferric state. Thus, sequential formation and decay of MPO Compound II occurred at sufficiently different rates to enable each process to be studied by conventional (i.e., single mixing) stopped-flow methods.

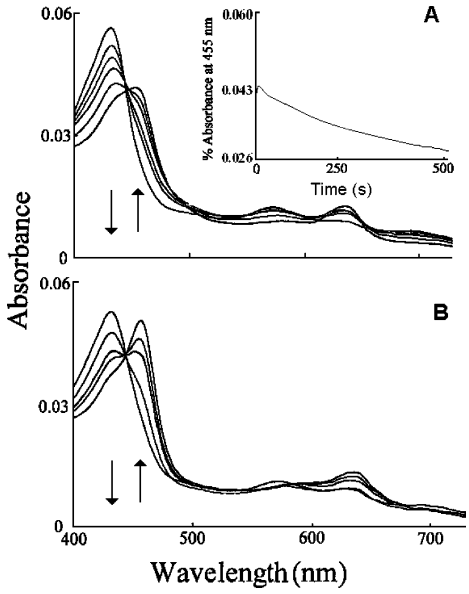

FIGURE 1: Time course of MPO Compound II formation following addition of H_2O_2 in the absence and in the presence of NO. An anaerobic solution containing sodium phosphate buffer (200 mM, pH 7.0) supplemented with H_2O_2 (40 μM) was rapidly mixed with an equal volume of buffer supplemented with 1.3 μM of MPO−Fe(III) and 200 μM SCN^- either in the absence (A) or in the presence (B) of NO (5 μM) at 10 °C. In A, spectral traces were collected at 0.1, 2, 5, 20, 42 s after initiating the reaction. In B, spectral traces were collected at 0.01, 0.042, 0.13, 0.2, and 0.5 s after initiating the reaction. Inset of panel A shows a stopped-flow trace collected in 500 s by monitoring the spectral changes at 455 nm, a characteristic wavelength for Compound II.

We next utilized single wavelength stopped-flow spectroscopy to investigate how NO interacted with MPO Compound II and the MPO−Fe(III) states during steady-state catalysis of SCN^-. The influence of NO on the kinetics of MPO Compound II build-up, duration, and decay were examined under anaerobic conditions following rapid mixing of the enzyme solution preincubated with 200 μM SCN^- in the presence of increasing concentrations of NO (e.g., 5, 10, 20, and 40 μM) against 40 μM H_2O_2. Figure 2 shows actual stopped-flow traces (indicated by the filled circles) collected at 455 nm in the presence of various NO concentrations, along with their computer simulation (solid lines) using

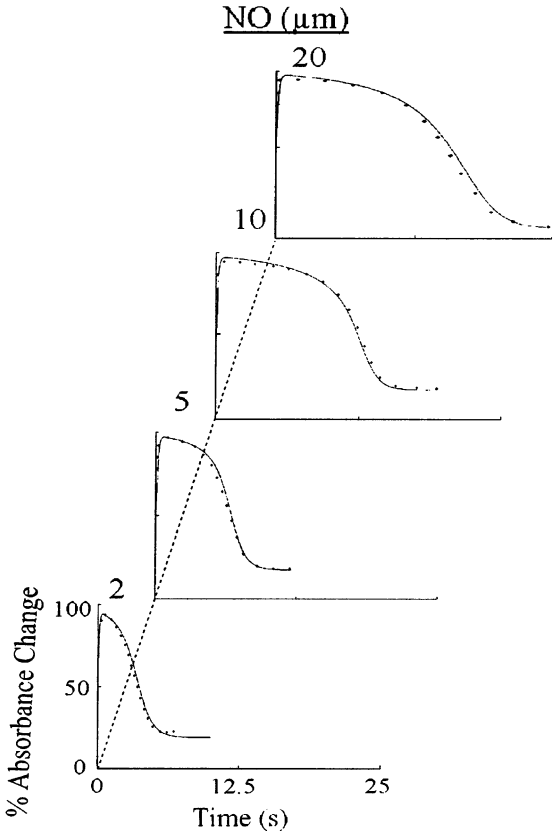

FIGURE 2: Effect of NO concentration on MPO Compound II formation, duration, and decay during steady-state metabolism of SCN^-. Formation and decay of Compound II of MPO was monitored as a function of time by observing spectral changes at 455 nm (●). An anaerobic solution containing sodium phosphate buffer (200 mM, pH 7.0) supplemented with H_2O_2 (40 μM) was rapidly mixed with an equal volume of buffer containing 1 μM of MPO−Fe(III), 200 μM SCN^-, and differing concentrations of NO at 10 °C. The final concentration of NO in mixtures is indicated in micromolar. The symbols represent portions of the experimental data, while the solid lines represent the simulated time courses using the rate constants that appear in the results section and the model in Scheme 1.

methods and kinetic constants as previously described (*10*, *15*−*18*, *26*, *27*, *38*−*41*). When the same reactions were monitored at 432 nm, the direction of absorbance changes was reversed and the signal amplitudes increased (data not shown), but otherwise, proceeded with identical kinetics (Figure 3). Figure 3 shows the relationship between NO concentration and the rate of MPO Compound II formation (upper panel), its duration as determined by the time elapsed during catalysis (middle panel), and the rate of steady-state depletion (lower panel). It was evident that as the NO concentration increased both the rate constant of MPO Compound II formation and its elapsed time progressively increased in linear and saturable manners. The MPO Compound II steady-state depletion rate remained relatively constant across the NO concentration range examined (Figure 3, lower panel).

Understanding how NO influences the mechanism of MPO and modulates its productivity during catalysis will help us understand why the MPO Compound I prefers to undergo a one rather than a two e^- oxidation pathway following interaction with the cosubstrates. To assess whether the model presented in Scheme 1 is reasonable, we performed computer simulations of the obtained experimental results.

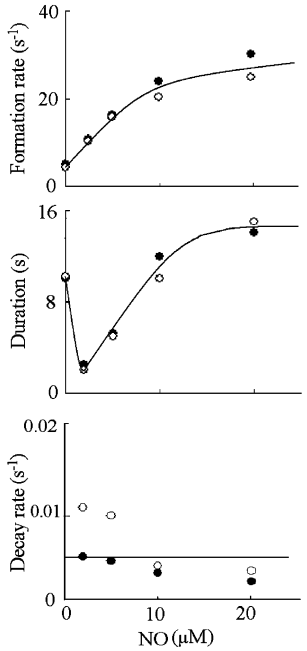

FIGURE 3: Rate of MPO Compound II formation, duration, and decay as a function of NO concentration. The observed rate of MPO Compound II formation (upper panel), duration (middle panel), and decay (lower panel) (monitored at 455 nm) observed in Figure 2 were plotted as a function of NO concentration. Data represent the mean of triplicate determinations from an experiment performed three times. The open circles represent kinetic parameters collected at 455 nm, while the closed circles represent kinetic parameters collected at 432 nm.

Numeric integration of the partial differential equations describing the reactions was used in the computer simulations (*10*, *15*−*18*, *26*, *27*, *31*−*41*). The rate constants used in the simulations were either previously reported (temperature corrected) or derived from the measurements reported here and are listed below.

k_1: The reaction between MPO−Fe(III) and hydrogen peroxide was given a rate constant of 6.00×10^6 s^{-1} M^{-1}, as previously reported (*38*).

k_{-1}: The reverse rate constant for decay of Compound I back to the ferric state was given a value of 26 s^{-1} (*38*).

k_2: The rate constant for the $2e^-$ oxidation of SCN^- by MPO Compound I was assigned a value of 8.0×10^7 M^{-1} s^{-1} (*42*).

k_3: The rate constant for the conversion of Compound I to Compound II was given a value of 3.00×10^4 s^{-1}. A great variety of electron donors mediate this transformation including H_2O_2 (*38*).

k_4: The rate constant for the conversion of Compound I to the Compound II in the presence of excess SCN^- was given a value of 5.0 M^{-1} s^{-1}, as recently reported (*26*).

k_5: The conversion of Compound I to the Compound II in the presence of NO was given a rate constant of 7.0×10^6 M^{-1} s^{-1} (*16*).

k_6: The conversion of Compound II* to Compound II was given a rate constant of 1.98 s^{-1}.

k_{-6}: The reversed rate constant for the conversion of Compound II* to Compound II was assigned a value of 0.50 s^{-1}.

k_7: Decay of Compound II to the ferric state was given a rate constant of 0.008 s^{-1} (*15*).

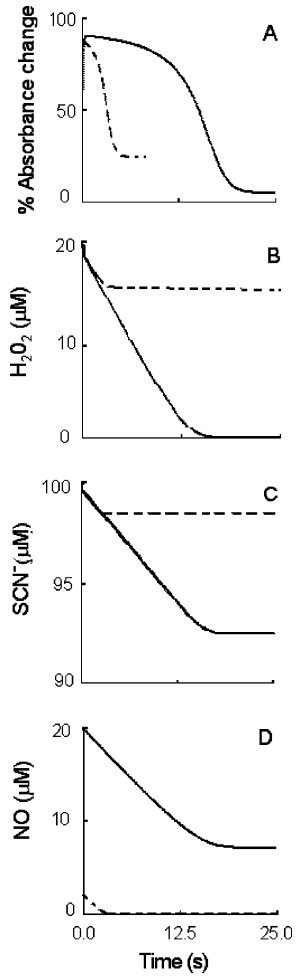

FIGURE 4: Computer simulation of the reactions depicted in Scheme 1. (A) Simulated time courses for the progression of the reaction of MPO preincubated with SCN^- when the reaction was monitored at 455 nm in the presence of 2 μM (- - -) and 20 μM (—) NO. Panels B, C, and D apply to H_2O_2, SCN^-, and NO consumption for the same reactions, respectively.

k_8: The conversion of Compound II to the ferric state in the presence of NO was given a rate constant of 5.0×10^6 M^{-1} s^{-1} (*16*).

k_9: Formation of the MPO−Fe(III)−NO complex was given a rate constant of 1.07×10^6 M^{-1} s^{-1}, as previously experimentally determined (*15*).

k_{-9}: Dissociation of NO from the MPO−Fe(III)−NO complex was assigned an experimental value of 15 s^{-1} (*15*).

k_{10}: MPO−Fe(III) reaction with SCN^- present in excess in the solution was given a rate constant of 9.0×10^5 M^{-1} s^{-1}, as previously reported (*43*). In this reaction, we assume that SCN^- behaves as a substrate (*43*).

k_{-10}: Dissociation of SCN^- from the SCN−MPO−Fe(III) complex was assumed to have a rate constant of 45 s^{-1}.

k_{11}: Experimentally determined value of 5.00×10^5 M^{-1} s^{-1} at 10 °C for the formation of the SCN-MPO−Fe(III)−NO complex was used in the computer simulation (*26*).

k_{-11}: Dissociation of NO from the SCN−MPO−Fe(III)−NO complex was given a rate constant of 25 s^{-1} (*26*).

The initial concentrations of SCN^- and MPO were 200 and 1 μM, respectively. The simulation of the reactions in Scheme 1, shown in Figure 2, qualitatively accounts for all of our experimental observations—specifically, the formation, duration, and decay of MPO Compound II. We were unable to simulate all the time courses without including a conformational step that limits the decay of Compound II to the ferric state. We have, therefore, incorporated into the model a second form of MPO Compound II (Scheme 1). By including this step, together with the other steps depicted in the model, we have been able to accurately simulate the time courses for the catalytic reactions of MPO as a function of NO concentrations. All rate constants were kept fixed and obtained from the current studies, or as previously reported, except k_6 and k_{-6}, which were first estimated graphically until the simulated time courses matched the experimental data. The stopped-flow traces, along with their corresponding simulated traces obtained by fitting the data to Scheme 1, are shown in Figure 2. The kinetic simulation traces were obtained by direct comparison of the experimental and calculated time courses for intermediate and product formation using Reaction Kinetics software.

Figure 4A shows the simulated time courses of MPO Compound II at two different NO concentrations, 2 and 20 μM. The majority of the enzyme converted to Compound II during the initial phase of the reaction and remained at the same level through the progress of the reaction until all the H_2O_2 or the NO was depleted (Figure 4). Consumption of SCN^- and NO was linear according to the model and ceased when H_2O_2 or NO was completely consumed (Figure 4B−D). The kinetic simulation also revealed that the amount of SCN^- consumed by MPO was significantly increased upon increasing NO concentration (Figure 4C).

DISCUSSION

Our results suggest a complex and interdependent relationship between NO levels and MPO catalytic activity and function during the steady-state metabolism of SCN^-. NO displays the potential capacity to influence the formation rate, the percentage of MPO Compound II formed (amplitude of the 455 nm signal), the time of the reaction (duration of the 455 nm signal), and the decay rate during SCN^- metabolism. NO dramatically modulates levels of MPO Compound II during catalysis; the MPO Compound II formation rates increased in a nearly linear manner and showed signs of saturating only when NO concentrations reached 10 μM, while the decay rates proceeded independently of NO concentration. This mechanistic feature suggests that under physiological conditions, in which the presence of both SCN^- and NO during MPO Compound II catalysis is anticipated, the presence of NO promotes a conformational change that can greatly limit the MPO Compound II decay rate to the ferric state. Such behavior is corroborated by computer simulation of our experimental data using rate constants previously reported (*10*, *15*−*18*, *26*, *27*, *38*−*41*) and the model, which appears in Scheme 1. These simulation traces approximate what was observed experimentally and suggest the involvement of a conformational intermediate of MPO Compound II complex decay. Collectively, our results support the notion that the presence of NO may participate in promoting substrate switching by steering the reaction from the $2e^-$ to the $1e^-$ oxidation pathway during SCN^- metabolism. These findings display an important application in biological systems, since alteration in NO levels is a characteristic feature of many inflammatory and cardiovascular diseases.

Recent studies have demonstrated that preincubation of mammalian peroxidase superfamily enzymes with SCN^- modulates their catalytic activity and function by serving as a substrate or an inhibitor (*26*, *41*, *44*−*49*). Rapid kinetic measurements have revealed that the characteristic mechanistic properties of MPO Compound II are similar to those of EPO but distinct from that of LPO (*26*). MPO Compound II accumulation during the steady-state metabolism of SCN^- allows the enzyme to function at only a fraction of its maximum catalytic activity in generating the corresponding hypohalous acid, since MPO Compound II does not possess suitable redox potential to oxidize SCN^- by $1e^-$ (*26*). Because the rate of MPO Compound I decay significantly exceeds its rate of formation when the enzyme was preincubated with SCN^- (e.g., 200 μM) (*10*, *27*, *38*−*41*), Compound I accumulation could not be seen. Instead, the second slower reaction could be monitored, which, in this case, is the accumulation, duration, and decay of Compound II. Consistent with this hypothesis, rates of spectral changes as a function of wavelength of MPO were invariant, and both processes (Compound II formation vs Compound II decay) generate a single set of spectral isosbestic points. This behavior indicates that MPO Compound II formation and decay occur without the accumulation of other spectroscopically observed intermediates, which is also the case for the metabolism of SCN^- in the absence of NO (*26*).

NO has been shown to play a different role in each step of MPO catalysis (*15*−*18*). In the presence of biologically relevant levels of NO ($\leq$2.5 μM) and SCN^- (100 μM), NO predominantly serves as a $1e^-$ reductant for MPO Compounds I and II, as reflected in an enhancement of MPO Compound II accumulation and accelerated rates of complex formation and decay. The presumed intermediate formed, nitrosonium cation (NO^+), is remarkably unstable and is rapidly hydrolyzed in aqueous solutions yielding nitrite (NO_2^-). As NO concentrations were increased, we observed a significant increase in the rate of Compound II formation, which correlated with proportional increases in the duration of the reaction as determined by the time elapsed during steady-state catalysis (Figures 2 and 3). At higher levels of NO (i.e., when NO levels are higher than the K_{diss} for Fe(III)−NO), NO predominantly serves as a ligand for the MPO−Fe(III) form, generating its inactive Fe(III)−NO complex (Scheme 1) (*15*−*18*). Remarkably, bound SCN^- modulates NO binding to the heme iron. The second-order rate constant plotted as a function of SCN^- showed a bell-shaped relationship with a trough centered at the plasma levels of SCN^- (*26*). This behavior is physiologically relevant and may indicate that SCN^- binding modulates the rate of H_2O_2 binding to MPO− heme iron, and subsequently, modulates the catalytic activity of the enzyme. At low SCN^- concentration, SCN^- binds to the distal cavity located in MPO Compound I and allows the direct contact with the oxyferryl oxygen (*47*−*49*). Under these circumstances, Compound I is a very strong oxidant that can be reduced by SCN^- to produce hypothiocyanate as a final reaction product (*47*−*49*). At a higher SCN^- concentration, SCN^- binds to MPO at both the distal cavity and the proximal helix sites and forms an inactive complex. Therefore, the dissociation rates of NO from MPO−Fe(III)−NO and the cleavage of SCN^- from SCN−MPO−Fe(III) also account for the differences in the observed plots of NO concentration vs rate of Compound II formation for the enzyme (Scheme 1). Thus, the rate-limiting step at high levels of NO and SCN^- shifts from reduction of Compound II to dissociation of these molecules from their corresponding complexes (Scheme 1). Since the SCN^- is kept constant at all NO concentrations used, the plot plateaus at a rate comparable to the dissociation rate constant for the respective Fe(III)−NO complexes.

To further investigate why the changes in NO concentration did not affect the decomposition of MPO Compound II to the ferric state and to evaluate our kinetic model, we performed computer simulations of the reactions shown in Scheme 1. This scheme is based on the known intermediates in the reaction sequence, as well as the proposed Compound II conformational intermediate that limits the MPO Compound II decay rate. This conformational change is slow enough to kinetically be the rate-limiting step in the decay process. It may play an important factor in promoting the increase in the duration, increase in the amplitude of MPO Compound II, and the unaltered proportional decay rates upon increasing NO concentration. Computer simulation shows that the majority of MPO was rapidly converted to Compound II during the initial phase of the reaction, and remained at a nearly constant level during catalysis until all the H_2O_2 or the NO was depleted (Figure 4). The build-up of Compound II that occurs in the first milliseconds of initiating the reaction was accompanied by an approximately 40-fold decrease in the rate of H_2O_2 reduction, as indicated by a deflection in the rate of H_2O_2 consumption to a slower rate (Figure 4B). The first phase of the reaction can be attributed to H_2O_2 oxidation of MPO ferric state, which precedes formation of Compound I. The subsequent decrease in the rate of all H_2O_2 consumption can be attributed to the formation and accumulation of MPO Compound II, the rate limiting step in the peroxidase cycle. In parallel, NO consumption continues linearly until all the H_2O_2 was depleted. After H_2O_2 or NO was exhausted, the Compound II signal decayed over a 3 s period. The amount of SCN^- consumed by MPO is significantly increased upon increasing NO concentration (Figure 4C,D). Thus, the kinetic data suggest that the build-up of the catalytic metabolism of SCN^- and Compound II formation, duration, and decay is a reaction driven by NO. As is illustrated in Scheme 1, the degree of Compound II formation during the metabolism of SCN^- likely depends on several factors, primarily the rate of SCN^- reduction through $2e^-$ versus $1e^-$ pathways, the concentration of NO versus SCN^-, the extent of Fe(III)−NO complex formation, and the complex breakdown. Our spectral data, combined with computer simulation results, show that very little MPO exists as Compound I during the steady-state metabolism of SCN^-.

To summarize, the present studies demonstrate a potential role of NO in influencing the metabolism of SCN^- by MPO (Scheme 1). Previously, we have shown that the build-up of MPO Compound II during steady-state catalysis of SCN^- allows the enzyme to function at only a fraction of its maximum activity in generating the corresponding hypohalous acid. Using a combination of biochemical and kinetic approaches, we now show that NO upregulates the overall catalytic activity of MPO by destabilizing MPO Compound II, a process mediated by direct interaction of NO as a peroxidase substrate, and enhances overall rates of catalysis (*18*). This process may also modulate the distribution of

peroxidase intermediates, Compounds I and II, available during steady-state catalysis, hence, affecting the substrate selectivity of the enzymes and promoting "substrate switching" for the peroxidases by influencing the ability of $1e^-$ vs $2e^-$ reducing substrates to undergo catalysis.

REFERENCES

1. Klebanoff, S. J., and Clark, R. A. (1987) *The Neutrophil: Functions and Clinical Disorders*, pp 1−810, Elsevier Science Publisher B. V., Amsterdam.
2. Klebanoff, S. J. (2005) Myeloperoxidase: friend and foe, *J. Leukocyte Biol. 77*, 598−625.
3. Hazen, S. L., and Heinecke, J. W. (1997) 3-Chlorotyrosine, a specific marker of myeloperoxidase-catalyzed oxidation, is markedly elevated in low-density lipoprotein isolated from human atherosclerotic intima, *J. Clin. Invest. 99*, 2075−2081.
4. Podrez, E. A., Schmitt, D., Hoff, H. F., and Hazen, S. L. (1999) Myeloperoxidase-generated reactive nitrogen species convert LDL into an atherogenic form in vitro, *J. Clin. Invest. 103*, 1547−1560.
5. Thukkani, A. K., McHowat, J., Hsu, F., Brennan, M. L., Hazen, S. L., and Ford, D. A. (2003) Identification of alpha-chloro fatty aldehydes and unsaturated lysophosphatidylcholine molecular species in human atherosclerotic lesions, *Circulation 108*, 3128−3133.
6. Nicholls, S. J., and Hazen, S. L., (2005) Myeloperoxidase and cardiovascular disease, *Arterioscler. Thromb. Vasc. Biol. 25*, 1102−1111.
7. Brennan, M. L., Penn, M. S., Van Lente, F., Nambi, V., Shishehbor, M. H., Aviles, R. J., Goormastic, M., Pepoy, M. L., McErlean, E. S., Topol, E. J., Nissen, S. E., and Hazen, S. L. (2003*)* Prognostic value of myeloperoxidase in patients with chest pain, *N. Engl. J. Med. 349*, 1595−1604.
8. Weiss, S. J., Klein, R., Slivka, A., and Wei, M. (1982) Chlorination of taurine by human neutrophils. Evidence for hypochlorous acid generation, *J. Clin. Invest. 70*, 589−607.
9. Harrison, J. E., and Schultz, J. (1976) Studies on the chlorinating activity of myeloperoxidase, *J. Biol. Chem. 251*, 1371−1374.
10. Kettle, A. J., van Dalen, C. J., and Winterbourn, C. C. (1997) Peroxynitrite and myeloperoxidase leave the same footprint in protein nitration, *Redox Rep. 3*, 257−258.
11. Klebanoff, S. J. (1999) Myeloperoxidase, *Proc. Assoc. Am. Physicians 111*, 383−389.
12. Podrez, E. A., Abu-Soud, H. M., and Hazen, S. L. (2000) Myeloperoxidase-generated oxidants and atherosclerosis, *Free Radical Biol. Med. 28*, 1717−1725.
13. Nauseef, W. M. (1998) Insights into myeloperoxidase biosynthesis from its inherited deficiency, *J. Mol. Med. 76*, 661−618.
14. Petrides, P. E., and Nauseef, W. M. (2000) *The Peroxidase Multi-Gene Family of Enzymes: Biochemical* Basis and Clinical Applications (Petrides, P. E., and Nauseef, W. M., Eds.), Springer-Verlag, Berlin, Germany.
15. Abu-Soud, H. M., and Hazen, S. L. (2000) Nitric oxide modulates the catalytic activity of myeloperoxidase, *J. Biol. Chem. 275*, 5425−5430.
16. Abu-Soud, H. M., and Hazen, S. L. (2000) Nitric oxide is a physiological substrate for mammalian peroxidases, *J. Biol. Chem. 275*, 37524−37532.
17. Abu-Soud, H. M., Khassawneh, M. Y., Sohn, J. T., Murray, P., Haxhiu, M. A., and Hazen, S. L. (2001) Peroxidases inhibit nitric oxide (NO) dependent bronchodilation: development of a model describing NO-peroxidase interactions, *Biochemistry 40*, 11866−11875.
18. Galijasevic, S., Saed, G. M., Diamond, M. P., and Abu-Soud, H. M. (2003) Myeloperoxidase up-regulates the catalytic activity of inducible nitric oxide synthase by preventing nitric oxide feedback inhibition, *Proc. Natl. Acad. Sci. U.S.A. 100*, 14766−14771.
19. van Dalen, C. J., and Kettle, A. J. (2001) Substrates and products of eosinophil peroxidase, *Biochem. J. 358*, 233−239.
20. Winterbourn, C. C., and Kettle, A. J. (2004) Reactions of superoxide with myeloperoxidase and its products, *Jpn. J. Infect. Dis. 57*, S31−S33.
21. Nielsen, F. H. (1986) in *Trace Elements in Human and Animal Nutrition* (Mertz, W., Ed.) Vol. 2, pp 426−430, Academic Press, Orlando, FL.
22. van Dalen, C. J., Whitehouse, M. W., Winterbourn, C. C., Kettle, A. J. (1997) Thiocyanate and chloride as competing substrates for myeloperoxidase, *Biochem. J. 327*, 487−492.
23. Teitz, N. W. (1994) *Teitz Textbook of Clinical Chemistry* (Burtis, C. A., and Ashwood, E. R., Eds.) 2nd ed., p 2216, W. B. Saunders Co., Philadelphia, PA.
24. Thomas, E. L., Bozeman, P. M., Jefferson, M. M., and King, C. C. (1995) Oxidation of bromide by the human leukocyte enzymes myeloperoxidase and eosinophil peroxidase. Formation of bromamines, *J. Biol. Chem. 270*, 2906−2913.
25. van der Vliet, A., Eiserich, J. P., Halliwell, B., and Cross, C. E. (1997) Formation of reactive nitrogen species during peroxidase-catalyzed oxidation of nitrite. A potential additional mechanism of nitric oxide-dependent toxicity, *J. Biol. Chem. 272*, 7617−7625.
26. Tahboub, Y. R., Galijasevic, S., Diamond, M. P., and Abu-Soud, H. M. (2005) Thiocyanate modulates the catalytic activity of mammalian peroxidases, *J. Biol. Chem. 280*, 26129−26136.
27. Furtmuller, P. G., Burner, U., Regelsberger, G., and Obinger, C. (2000) Spectral and kinetic studies on the formation of eosinophil peroxidase compound I and its reaction with halides and thiocyanate, *Biochemistry 39*, 15578−15584.
28. Azen, E. A. (1978) Salivary peroxidase activity and thiocyanate concentration in human subjects with genetic variants of salivary peroxidase, *Arch. Oral Biol. 23*, 801−805.
29. Ferguson, D. B. (1987) Current diagnostic uses of saliva, *J. Dent. Res. 66*, 420−424.
30. Stevens, K. R., and Munoz, L. R. (2004) Cigarette smoking: Evidence to guide measurement, *Res. Nurs. Health 27*, 281−292.
31. Scherer, G., and Richter, E. (1997) Biomonitoring exposure to environmental tobacco smoke (ETS): a critical reappraisal, *Hum. Exp. Toxicol. 16*, 449−459.
32. Bottoms, S. F., Kuhnert, B. R., Kuhnert, P. M., and Reese, A. L. (1982) Maternal passive smoking and fetal serum thiocyanate levels, *Am. J. Obstet. Gynecol. 144*, 787−791.
33. McMahon, M. J., Brown, H. L., and Dean, R. A. (1997) Umbilical cord thiocyanate and thyroid function in intrauterine growth-restricted infants of the smoking gravida, *J. Perinatol. 17*, 370−374.
34. Thayer J. R., and Huffaker, R. C. (1980) Determination of nitrate and nitrite by high-pressure liquid chromatography: comparison with other methods for nitrate determination, *Anal. Biochem. 102*, 110−119.
35. Rakita, R. M., Michel, B. R., and Rosen, H. (1990) Differential inactivation of *Escherichia coli* membrane dehydrogenases by a myeloperoxidase-mediated antimicrobial system, *Biochemistry 29*, 1075−1080.
36. Wever, R., Plat, H., and Hamers, M. N. (1981) Human eosinophil peroxidase: a novel isolation procedure, spectral properties and chlorinating activity. Kinetics of oxidation of tyrosine and dityrosine by myeloperoxidase compounds I and II. Implications for lipoprotein peroxidation studies, *FEBS Lett. 123*, 327−331.
37. Agner, K. (1963) Studies on myeloperoxidase activity, *Acta Chem. Scand. 17*, S332−S338.
38. Marquez, L. A., and Dunford, H. B. (1995) Kinetics of oxidation of tyrosine and dityrosine by myeloperoxidase compounds I and II. Implications for lipoprotein peroxidation studies, *J. Biol. Chem. 270*, 30434−30440.
39. Arnhold, J., Furtmuller, P. G., and Obinger, C. (2003) Redox properties of myeloperoxidase, *Redox Rep.* 8, 179−186.
40. Dunford, H. B., and Hsuanyu, Y. (1999) Kinetics of oxidation of serotonin by myeloperoxidase compounds I and II, *Biochem. Cell Biol. 77*, 449−457.
41. Stelmaszynska, T., and Zgliczynski, J. M. (1974) Myeloperoxidase of human neutrophilic granulocytes as chlorinating enzyme, *Eur. J. Biochem. 45*, 305−312.
42. Furtmuller, P. G., Burner, U., and Obinger, C. (1998) Reaction of myeloperoxidase compound I with chloride, bromide, iodide, and thiocyanate, *Biochemistry 37*, 17923−17930.
43. Ghibaudi, E., Laurenti, E., Pacchiardo, C., Suriano, G., Moguilevsky, N., Pia Ferrari, R. (2003*)* Organic and inorganic substrates as probes for comparing native bovine lactoperoxidase and recombinant human myeloperoxidase, *J. Inorg. Biochem. 94*, 146−154.
44. Zgliczynski, J. M., Selvaraj, R. J., Paul, B. B, Stelmaszynska, T., Poskitt, P. K., and Sbarra, A. J. (1977) Chlorination by the myeloperoxidase-H_2O_2-Cl-antimicrobial system at acid and neutral pH, *Proc. Exp. Biol. Med. 154*, 418−422.

45. Bakkenist, A. R. J., de Boer, J. E., Plat, H., and Wever, R. (1980) The halide complexes of myeloperoxidase and the mechanism of the halogenation reactions, *Biochim. Biophys. Acta 613*, 337−348.

46. Andrews, P. C., and Krinsky, N. I. (1982) A kinetic analysis of the interaction of human myeloperoxidase with hydrogen peroxide, chloride ions, and protons, *J. Biol. Chem. 257*, 13240−13245.

47. Zeng, J., and Fenna, R. E. (1992) X-ray crystal structure of canine myeloperoxidase at 3 Å resolution, *J. Mol. Biol. 226*, 185−207.

48. Fiedler, T. J., Davey, C. A., and Fenna, R. E. (2000) X-ray crystal structure and characterization of halide-binding sites of human myeloperoxidase at 1.8 Å resolution, *J. Biol. Chem. 275*, 11964−11971.

49. Davey, C. A., and Fenna, R. E. (1996) 2.3 Å resolution X-ray crystal structure of the bisubstrate analogue inhibitor salicylhydroxamic acid bound to human myeloperoxidase: a model for a prereaction complex with hydrogen peroxide, *Biochemistry 35*, 10967−10973.

BI051438K